Journal of Fluids and Structures 77 (2018) 170–181

Contents lists available at ScienceDirect

Journal of Fluids and Structures

journal homepage: www.elsevier.com/locate/jfs

Numerical study of vortex-induced vibrations of a flexible cylinder in an oscillatory flow

Bowen Fu, Lu Zou, Decheng Wan *

State Key Laboratory of Ocean Engineering, School of Naval Architecture, Ocean and Civil Engineering, Shanghai Jiao Tong University, Collaborative Innovation Center for Advanced Ship and Deep-Sea Exploration, Shanghai 200240, China

HIGHLIGHTS

- VIV of a flexible cylinder in an oscillatory flow is simulated using a CFD method;
- In-line vibrations are found to consist of three components;
- The butterfly-shaped trajectory has been observed;
- Wavelet analyses of vibrations and hydrodynamic forces have been conducted.

ARTICLE INFO

Article history:
Received 15 May 2017
Received in revised form 13 October 2017
Accepted 1 December 2017

Keywords:
Vortex-induced vibration
Oscillatory flow
Flexible cylinder
Viv-FOAM-SJTU solver
Fluid–structure interactions

ABSTRACT

The vortex-induced vibrations of a flexible cylinder oscillating harmonically in still water have been numerically simulated using a CFD method based on the strip theory. The algorithm PIMPLE in OpenFOAM is adopted to compute the flow field while the small-displacement Bernoulli–Euler bending beam theory is used to model the cylinder. Two ends of the flexible cylinder are forced to oscillate harmonically. The simulation results have been compared with experimental results and further analyzed. Features such as the hysteresis phenomenon and the build-up–lock-in–die-out cycle are observed in the cross-flow vibration. The in-line vibrations consist of three components, the low-frequency oscillation, the first-natural-frequency vibration during the cylinder reversal, and the second-natural-frequency vibration due to vortex shedding. The butterfly-shaped trajectory has been observed. Detailed wavelet analyses of the vibrations have been given at the end.

1. Introduction

A cylinder exposed to an oscillatory flow will experience vortex shedding if the Reynolds number and the Keulegan–Carpenter number are not too small, resulting in periodic variations in the force components on the cylinder. One feature of the cylinder exposed to an oscillatory flow is that the return of shedding vortices towards the cylinder after the flow reversal may cause a sudden change in the hydrodynamic forces. The in-line displacements primarily oscillate at the frequency of support motion, while small high-frequency periodic fluctuations are superimposed on the low-frequency displacements. These high-frequency fluctuations are induced by vortex shedding and vortex motions around the cylinder due to flow reversals. The case also applies to the in-line hydrodynamic forces. Vibrations will be amplified when the natural frequency is close to any of these vibration components, low-frequency oscillations or high-frequency fluctuations. When the amplitudes of the in-line oscillations become large, the in-line motions may begin to influence the cross-flow vibrations (Lipsett and Williamson, 1991). The cross-flow vibrations are generally of larger amplitudes.

* Corresponding author.
E-mail address: dcwan@sjtu.edu.cn (D. Wan).

https://doi.org/10.1016/j.jfluidstructs.2017.12.006
0889-9746/

Nomenclature

$\boldsymbol{\phi}$	Mode shape
A_y	Amplitude of cross-flow vibration
C_{Hx}	In-line hydrodynamic force coefficient
C_{Hy}	Cross-flow hydrodynamic force coefficient
D	Diameter of the cylinder
f_{Hx}	In-line hydrodynamic force frequency
f_{Hy}	Cross-flow hydrodynamic force frequency
f_{n1}	First natural frequency
f_{n2}	Second natural frequency
f_{st}	Strouhal frequency
f_s^m	Frequency of modal weight of variable s
f_w	Support motion frequency
f_x	In-line vibration frequency
f_y	Cross-flow vibration frequency
L	Length of the cylinder
$\bar{s}$	Time-averaged value of the variable s
s_{max}	Maximum value of the variable s
T	Tension of the cylinder
T_w	Support motion period
U_r	Reduced velocity
w_s^m	Modal weight of variable s
x	Relative in-line displacement
x_s	Support motion displacement
x_t	Total in-line displacement
y	Cross-flow displacement
z	Elevation

The hydrodynamic excitation of cylinders in oscillatory flows has been the subject of numerous investigations in the past several decades. Some researchers conducted experiments on the hydrodynamic response of rigid cylinders in oscillating flow (Kozakiewicz et al., 1994; Sarpkaya, 1979; Sumer and Fredsøe, 1988). From the experiment one of the typical characteristics of the response in oscillatory flows is the multi-peak behavior in the cross-flow amplitude responses (Kozakiewicz et al., 1997; Sumer and Fredsøe, 1988). A comprehensive review of the investigations can be found in Sumer and Fredsøe (1997). Some numerical investigations have also been conducted. Graham and Djahansouz (1991) used a discrete vortex method to predict the excitation of a cylinder in two directions. Anagnostopoulos and Iliadis (1998) used a finite element technique to study the cylinder response in the in-line direction. And more recently, Zhao (2013) conducted two-dimensional numerical studies of 2dof VIV of a circular cylinder in oscillatory flows, which reproduced some phenomena observed in experiments.

There is no much research on vortex-induced vibrations of flexible cylinders in oscillatory flows. Wang et al. (2014) conducted a series of experiments on this problem. In the present work, we investigate vortex-induced vibrations of a flexible cylinder subject to oscillatory flows using a computational fluid dynamics method, with parameters maintained identical to the model test by Wang et al. (2014) to facilitate comparison. The simulations are based on the in-house solver viv-FOAM-SJTU, which has been validated in previous studies (Duan et al., 2016; Fu et al., 2016; Wan and Duan, 2017). The present article is organized as follows. Section 2 introduces the concerned problems, followed by the simulation methods in Section 3 for handling the problems in Section 2. And Section 4 gives the simulation results with detailed analyses. Finally, a curt summary is presented in Section 5.

2. Problem

As regards oscillatory flows, there are two approaches to form them. In one, oscillatory flows are created by driving the water. For example, in the study of Sarpkaya (1986), a U-shaped oscillating flow tube was used. While in most other research, an oscillating cylinder is adopted. In both the experiment of Wang et al. (2014) and the present simulation, the oscillatory flow is formed by forcing two ends of the cylinder to oscillate harmonically. The main parameters of the experiment are listed in Table 1 and are maintained identical in the simulation. The mass ratio m^* in Table 1 denotes the ratio of the mass of the cylinder to the mass of the displaced water. Depicted in Fig. 1 is the experimental setup. The support motion is a periodic

Table 1
Main parameters in both Wang et al. (2014) and the present work.

	Symbols	Values	Units
Mass ratio	m^*	1.53	–
Diameter	D	0.024	m
Length	L	4	m
Bending stiffness	EI	10.5	N m^2
Tension	T	500	N
First natural frequency	f_{n1}	2.68	Hz
Second natural frequency	f_{n2}	5.46	Hz
Keulegan–Carpenter number	KC	84	–
Maximum reduced velocity	$U_{r\ max}$	4	–

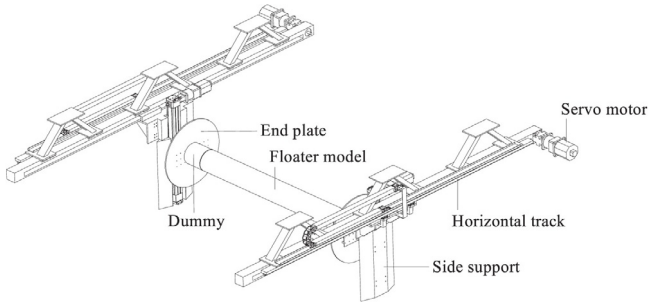

Fig. 1. Experimental setup in Wang et al. (2014). The supporting frame was forced to oscillate harmonically. The direction parallel to the support motion is referred to as the in-line direction x, while the direction perpendicular to the in-line direction x and the axial direction z is referred to as the cross-flow direction y.

function of time, expressed as

$$x_s = A \cdot \sin\left(\frac{2\pi}{T_w}t\right), \tag{1}$$

$$u_s = \frac{2\pi A}{T_w} \cdot \cos\left(\frac{2\pi}{T_w}t\right), \tag{2}$$

where A denotes the oscillating amplitude and T_w the oscillating period, x_s the oscillating displacement and u_s the oscillating velocity. The reduced velocity U_r of the support motion can be used to represent the relationship between the flow situations and the structural properties. It is supposed that the excitation range of cross-flow vibrations in terms of the reduced velocity extends over $3 < U_r < O(10)$ in water. In the present research, the maximum reduced velocity $U_{r\ max}$ can be written as

$$U_{r\ max} = \frac{u_{s\ max}}{f_{n1}D} = \frac{2\pi A}{T_w f_{n1} D}, \tag{3}$$

where f_{n1} is the first natural frequency of the cylinder. In the sinusoidal flow, the Keulegan–Carpenter (KC) number can be given by

$$KC = \frac{u_{s\ max} T_w}{D} = \frac{2\pi A}{D}, \tag{4}$$

in which $u_{s\ max}$ is the maximum support velocity. The physical meaning of the KC number can probably be best explained as the stroke of the motion to the diameter of the cylinder. Small KC numbers mean that the orbital motion of the water particles is small relative to the diameter of the cylinder. For very large KC numbers, we may expect that the flow for each half period of the motion resembles that in a steady current. The KC can be regarded as the dimensionless version of oscillating amplitude A.

3. Method

In order to compute the vibrations of flexible cylinders, the hydrodynamic forces acting on them must be obtained. To do this, the transient incompressible Reynolds-averaged Navier–Stokes equations are solved numerically:

$$\frac{\partial \overline{u_i}}{\partial x_i} = 0, \tag{5}$$

$$\rho\frac{\partial \overline{u_i}}{\partial t} + \rho\frac{\partial(\overline{u_i}\overline{u_j})}{\partial x_j} = -\frac{\partial \overline{p}}{\partial x_i} + \frac{\partial\left(2\mu\overline{S_{ij}} - \rho\overline{u_i' u_j'}\right)}{\partial x_j}, \tag{6}$$

where $\overline{S_{ij}}$ is the mean strain tensor

$$\overline{S_{ij}} = \frac{1}{2}\left(\frac{\partial \overline{u_i}}{\partial x_j} + \frac{\partial \overline{u_j}}{\partial x_i}\right), \tag{7}$$

and $\tau_{ij} = -\overline{u_i' u_j'}$ is the Reynolds stress tensor. The SST $k-\omega$ turbulence model is employed to determine the Reynolds stresses (Menter, 1994; Menter et al., 2003). No wall functions are used in the present work. Instead a refined mesh close to the cylinder is used to predict turbulence kinetic energy close to the cylinder (Chien, 1982; Wilcox, 1993).

Considering the large scale in the axial direction of the flow domain and also in the direction of support motion, it is not feasible to solve the three-dimensional flow field directly. In this case, a better choice is to solve two-dimensional flow strips located equidistantly along the span. As Willden and Graham (2004) has mentioned, though three-dimensional vortices might be developed when flow passes a cylinder, an effect of lock-in actually increases the correlation of flow along the span and renders the local flow primarily two-dimensional, making it possible to compute the fluid dynamics locally in a two-dimensional way. To some degree, the case also applies to oscillatory flows (Kozakiewicz et al., 1992). In order to reduce the computation cost and make the simulation feasible, 3-D features in the flow field are ignored in the present work. And the only connection between two strips is via cylinder displacements. Hydrodynamic forces are calculated from pressure forces and viscous forces integrated over the surface of the cylinder on each strip. The PIMPLE algorithm in the OpenFOAM is used to compute the two-dimensional flow fields (Holzmann, 2017).

On the other hand, the flexible cylinder is modeled as a small-displacement Bernoulli–Euler bending beam, with two ends set as pinned. In the present work, the two ends of the cylinder oscillate harmonically as prescribed. In contrast to steady currents, the concept 'in-line displacement' is not quite straightforward in oscillatory flows. Terms 'total in-line displacement' and 'relative in-line displacement' are used to distinguish the total one and the deflection. Thus, the cylinder's total displacement in the in-line direction is referred to as total in-line displacement x_t, i.e. the sum of the support motion x_s, plus the relative in-line displacement x:

$$x_t = x_s + x. \tag{8}$$

The equilibrium of forces for this system can be written as

$$m\ddot{x}_t + c\dot{x} + kx = f_{Hx}, \tag{9}$$

where m, c, k are the mass, the damping and the stiffness of the system, f_{Hx} the in-line hydrodynamic force. Thus we have

$$m\ddot{x} + c\dot{x} + kx = f_{Hx} - m\ddot{x}_s. \tag{10}$$

In the case of oscillatory flows, there is one additional contribution to the total in-line forces from the point of view of the cylinder, the additional inertial force. While in the direction vertical to the forced support motion, referred to as the cross-flow direction y, no such additional inertial force exists. In the finite element method the equations can be discretized as

$$\mathbf{M}\ddot{\mathbf{x}} + \mathbf{C}\dot{\mathbf{x}} + \mathbf{K}\mathbf{x} = \mathbf{F}_{Hx} - \mathbf{M}\ddot{\mathbf{x}}_s, \tag{11}$$

$$\mathbf{M}\ddot{\mathbf{y}} + \mathbf{C}\dot{\mathbf{y}} + \mathbf{K}\mathbf{y} = \mathbf{F}_{Hy}, \tag{12}$$

where $\mathbf{x}$, $\mathbf{x}_s$, and $\mathbf{y}$ are the relative in-line, the forced in-line, and the cross-flow nodal displacement vectors, the dot over a variable indicates its differentiation with respect to time, while $\mathbf{M}$, $\mathbf{C}$, $\mathbf{K}$ are the mass, the damping and the stiffness matrices. $\mathbf{F}_{Hx}$ and $\mathbf{F}_{Hy}$ are the hydrodynamic force vectors in corresponding directions. For the Rayleigh damping we have $\mathbf{C} = \alpha\mathbf{M} + \beta\mathbf{K}$, where α and β are calculated based on the first two natural frequencies f_{n1} and f_{n2} listed in Table 1, which are the actual involved ones, with the damping ratio ζ adopted as 0.03. The equation (Clough and Penzien, 2003) can be written as

$$\begin{bmatrix}\alpha \\ \beta\end{bmatrix} = \frac{2\zeta}{f_{n1} + f_{n2}}\begin{bmatrix}2\pi f_{n1} f_{n2} \\ 1/(2\pi)\end{bmatrix}. \tag{13}$$

Eqs. (11)–(12) are solved using the Newmark-beta method (Clough and Penzien, 2003).

With both the flow fields and the structure fields being solved separately, they can then be integrated together. At the beginning of each time level, the hydrodynamic forces are mapped to the structural model elements. Then the displacements of the cylinder are computed. With the displacements obtained, the mesh can be moved or deformed accordingly, thus resulting in new flow fields from which the hydrodynamic forces can be calculated. In this way, a time step is advanced. The procedure is shown in Fig. 2, based on which the solver viv-FOAM-SJTU is formed.

Twenty strips equidistantly located along the span of the cylinder are plotted in Fig. 3. These strips share the same initial flow field mesh, as shown in Fig. 4(a). The number of simulation strips can be determined by considering the highest mode of vibration. Three strips are required per half wave-length of vibration (Willden and Graham, 2004). The highest mode considered in the present work is the 2nd mode. As a result, 20 strips seem sufficient for the simulation. To verify the mesh resolution, meshes of 0.3, 0.5, 0.7 million cells have been tested. The results of 0.5 million cells differ only slightly with 0.7 million cells, especially in the low-frequency oscillations in the in-line hydrodynamic forces due to the support motion. Considering the randomness in the flow, it is reasonable for some variations to appear among the high-frequency forces.

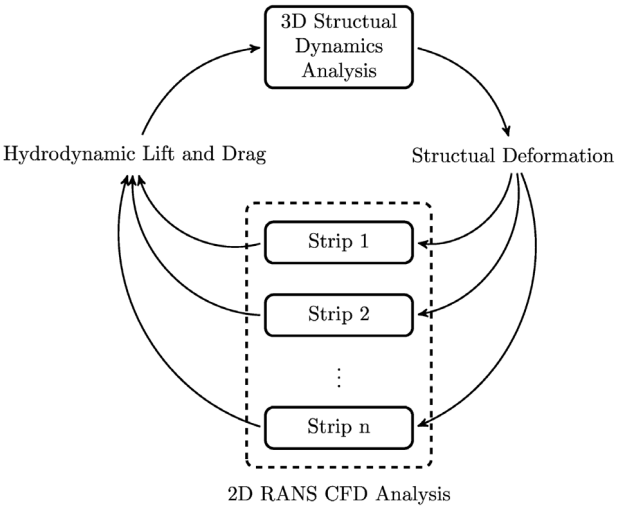

Fig. 2. Fluid–structure interaction. The fluid and the structure are coupled by hydrodynamic forces and structural displacements.

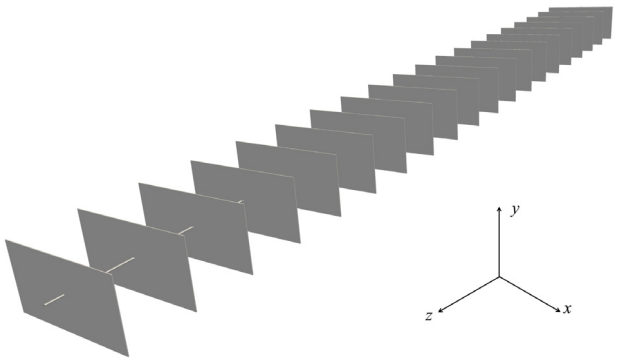

Fig. 3. Twenty strips located equidistantly along the span of the flexible cylinder.

The mesh of 0.5 million cells is employed for further investigation. The computation domain is of 80 cylinder diameters in the in-line direction x, 40 diameters in the cross-flow direction y. Every quadrant of the cylinder is divided into 40 parts. While 80 nodes are distributed in the radial direction between the cylinder and the outer concentric circle with a diameter 20 times that of the cylinder. The mesh near the cylinder is refined to predict turbulence kinetic energy close to it and is shown in Fig. 4(b). The motion solver "displacementLaplacian" in OpenFOAM is applied to handle the dynamic mesh (Jasak, 2009). Imposed on the surface of the cylinder is the no-slip boundary, and no external current is applied. The cylinder is discretized into 80 elements, with each element imposed of uniformly distributed loads.

4. Results

As has been mentioned above, cylinders tend to vibrate significantly for $3 < U_{\mathrm{r}} < O(10)$. In the present study, a case with the KC number of 84 and the maximum reduced velocity $U_{\mathrm{r\ max}}$ of 4 has been simulated (the oscillating period T_{w} is 7.5 s accordingly). The VIV development at the mid-span of the flexible cylinder in the cross-flow direction within half an oscillating period is presented in Fig. 5. The comparison between the present simulation and Wang et al. (2014) is given. To quantify the development of the cross-flow vibrations in the oscillatory flows, Wang et al. (2014) adopts the critical value of $\sqrt{2}/2$ of the maximum cross-flow displacement to define the 'lock-in' stage and the 'build-up' and 'die-out' stages. The 'lock-in' concept in the present study serves to characterize the intense vibration stage and is different from the generally accepted definition. The reduced velocity U_{r} increases over time in the build-up stage. As time passes the amplitude increases. When the amplitude exceeds the critical value mentioned above, the lock-in stage starts, during which the vibrations will reach the maximum amplitude in the half oscillating period. Similarly, when the amplitude falls below the critical value, the die-out stage starts and the amplitude will further decrease. It should be noted that the maximum amplitude appears not exactly at the reduced velocity peak, but shortly after it. For the selected half cycle, the lock-in duration is 21% of the half

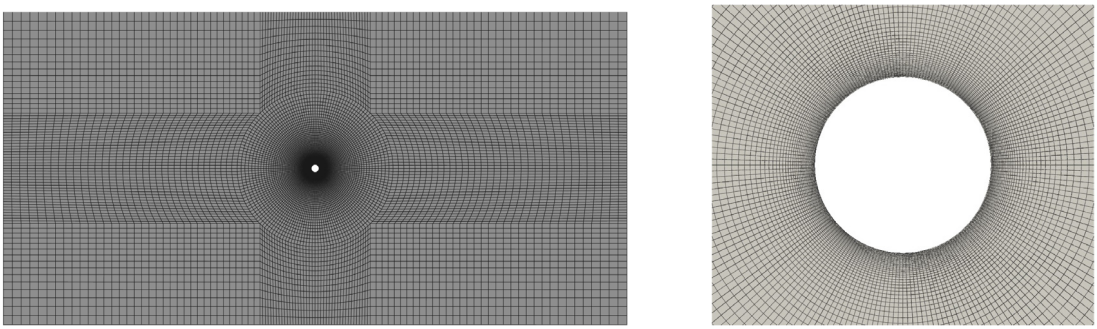

(a) Initial mesh on each strip. (b) Mesh near the cylinder.

Fig. 4. Mesh used in the simulation.

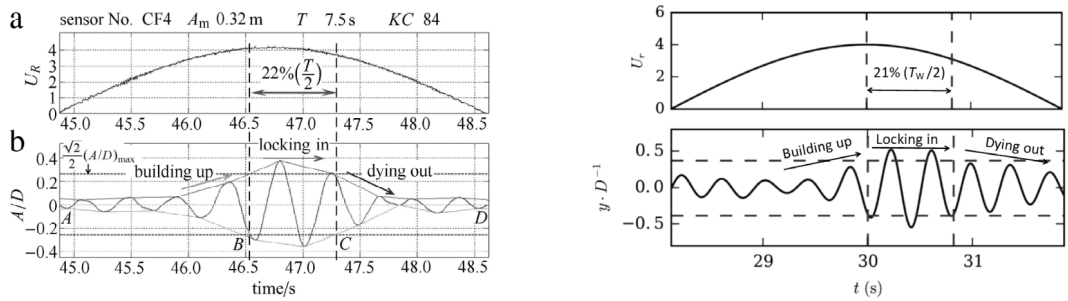

(a) Wang et al. (2014). (b) The present simulation.

Fig. 5. Development of the cross-flow vortex-induced vibrations at the mid-span of the cylinder within half an oscillating period.

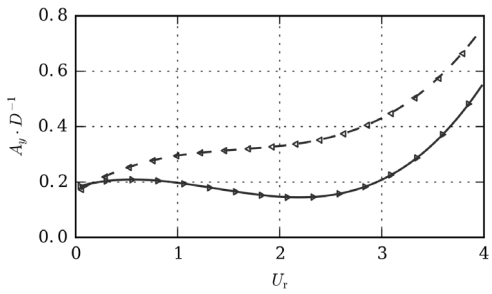

Fig. 6. Hysteresis phenomenon of cross-flow vibration amplitudes $A_y \cdot D^{-1}$ between accelerating and decelerating stages with the reduced velocity U_r varying from 0 to 4. The solid line with triangles pointing to right '▷' denotes the accelerating stages, while the dashed line with triangles pointing to left '◁' indicates the decelerating stages.

oscillating period $T_w/2$, while the value is 22% for Wang et al. (2014). From this perspective, the simulation agrees with the experiment well. The amplitude in the present simulation is slightly larger than that of the experiment. For in the absence of data of the damping ratio of the experimental model, the value of 0.03 is adopted. This small damping may give rise to the larger amplitude.

Oscillatory flows keep accelerating and decelerating by nature. It is not surprising to see that the response amplitudes in decelerating stages differ from those in accelerating stages with the same reduced velocities U_r, i.e. the hysteresis phenomenon occurs. In order to indicate the hysteresis phenomenon or the 'history dependence', the amplitudes of the cross-flow vibrations A_y varying with the reduced velocities U_r during the course of increase or decrease of the reduced velocity are obtained separately over a sufficiently long period of time, as plotted in Fig. 6, from which the differences between the accelerating and decelerating stages can be clearly seen. The 'hysteresis' means that the cross-flow vibration amplitudes A_y tend to be low in the early accelerating stages and are reluctant to be lowered down in decelerating stages. The lag between the vibration amplitude and the reduced velocity may be due to the lag between the vortex shedding (or the corresponding

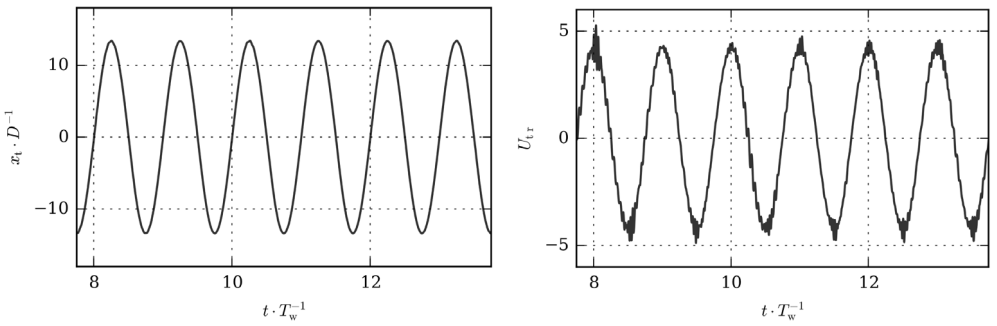

Fig. 7. The total in-line displacements $x_t \cdot D^{-1}$ and total in-line reduced velocities U_{tr} at the mid-span of the cylinder.

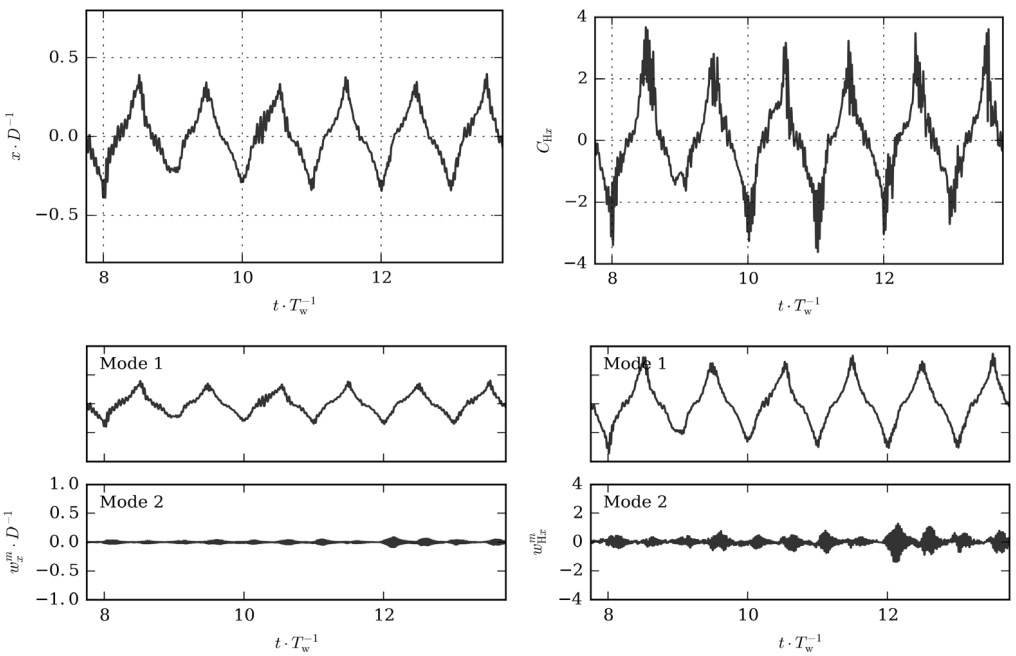

Fig. 8. The relative in-line displacements $x \cdot D^{-1}$ and the in-line hydrodynamic force coefficients C_{Hx} at the mid-span of the cylinder (upper) and modal weights of $x \cdot D^{-1}$ and C_{Hx} over the entire cylinder, $w_x^m \cdot D^{-1}$ and w_{Hx}^m (lower).

hydrodynamic forces on the flexible cylinder) and the reduced velocity. The vortex shedding doesn't change immediately when the velocity is altered.

The time t is non-dimensionalized by the oscillatory period T_w in the following analyses. Since $x_s = A \cdot \sin\left(2\pi\ t \cdot T_w^{-1}\right)$, the support displacement gets zero when $t \cdot T_w^{-1} = i + 0$ or 0.5, approaches peaks when $t \cdot T_w^{-1} = i + 0.25$, and approaches valleys when $t \cdot T_w^{-1} = i + 0.75$, where i is some integer. Thus this non-dimensionalization will largely facilitate analyses. The total in-line displacements and the total in-line reduced velocities at the mid-span of the cylinder are provided in Fig. 7 as a reference showing the situations and positions of the cylinder at any time in the selected interval.

Depicted in the upper part of Fig. 8 are time series of the relative in-line displacements at the mid-span of the cylinder and the corresponding hydrodynamic forces acting on it. There is a good deal of resemblance between the displacements and the forces. That is the result of the feedback between the responses and the forces. From the relative in-line displacement figure, it is clear that there exists a low-frequency, large-amplitude oscillation. The oscillation reaches its peaks and valleys when the support motion crosses zero, i.e. a lag of $0.25T_w$ seems to exist between the support motion and the low-frequency oscillation. It is known that there always exists a delay between the responses with the excitation forces. This delay is always a quarter of a period at the resonance, but negligible when the excitation frequency is far less than the natural frequency, which is exactly the case for the low-frequency oscillation. Thus, it is reasonable to assume that the low-frequency component of the in-line hydrodynamic forces caused by the support motion acts as the driving force of the low-frequency oscillation.

Another phenomenon is that when the support displacement $x_s \cdot D^{-1}$ reaches peaks or valleys (i.e. when the relative in-line displacement $x \cdot D^{-1}$ crosses zero), the distinct short-duration fluctuations manifest in the relative in-line displacements

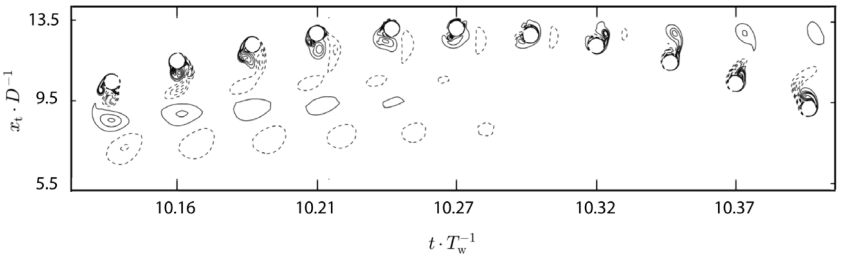

Fig. 9. Development of vortices during cylinder reversal in the strip at the mid-span of the cylinder. Horizontal axis: non-dimensionalized time $t \cdot T_w^{-1}$; vertical axis: total in-line displacements $x_t \cdot D^{-1}$.

$x \cdot D^{-1}$ and in-line hydrodynamic force coefficients C_{Hx}. When the cylinder reverses its motion direction, the vortices behind it will be washed over it. Plotted in Fig. 9 is the development of the vortices in the plane at the mid-span of the cylinder during the cylinder reversal. The short-duration fluctuations are attributed to the vortices washing over the cylinder.

The lower part of Fig. 8 presents the modal weights of the relative in-line displacements and the in-line hydrodynamic force coefficients. The deflected shape of the flexible cylinder is represented in spectral terms, i.e. the entire cylinder's displacements are decomposed into modal contributions in the least-squares sense (Lie and Kaasen, 2006; Trim et al., 2005) through

$$\boldsymbol{\phi}^{\mathbf{T}}\mathbf{x} = \boldsymbol{\phi}^{\mathbf{T}}\boldsymbol{\phi}\mathbf{w}_{\mathbf{x}}, \tag{14}$$

where only those desirable mode shapes are included in the matrix of mode shapes $\boldsymbol{\phi}$. Modal decompositions of forces are conducted in a similar way.

One feature of the in-line vibrations is that the first-order modal weight is mainly contributed by the hydrodynamic forces due to the support motion. And some fluctuations exist in the second-order modal weight shortly after the reduced velocity peaks or valleys. In the present case, the maximum Reynolds number $Re_{\max} = u_{s\ \max} D/\nu = 6174$, the flow is mainly in the 'subcritical' regime (Blevins, 2001). And the Strouhal number St for a smooth circular cylinder is about 0.2 in the 'subcritical' regime. The Strouhal number St is of the similar form to the reciprocal of the reduced velocity U_r,

$$St = \frac{f_{st} D}{u_s} = 0.2, \tag{15}$$

$$\frac{1}{U_r} = \frac{f_{n1} D}{u_s} \geq 0.25, \tag{16}$$

where f_{st} is the vortex shedding frequency for a stationary cylinder with the current speed u, i.e. the Strouhal frequency. When the cylinder is accelerating, the Strouhal number St gets closer to the reciprocal of the reduced velocity U_r, i.e. the Strouhal frequency f_{st} approximates the fundamental natural frequency of the flexible cylinder f_{n1}. When the Strouhal frequency gets close to the first natural frequency, the first-order modal weight of the cross-flow vibrations will increase. Accordingly, twice the Strouhal frequency will approximate the second natural frequency, i.e. the second-order modal weight of the in-line vibrations will increase, in exactly the same fashion as in steady currents. This is actually what we see from the lower part of Fig. 8 —the second-order modal weight manifests exactly after the reduced velocity peaks and valleys. Moreover, the second-order modal component of the in-line hydrodynamic forces seems more evident than that of the in-line displacements.

One way of determining the relationship between displacements and forces is to identify their dominant frequencies. A common technique regarding the determination of the dominant frequencies is Fourier analysis. Fourier analyses of modal weights of the in-line displacements and force coefficients are presented in Fig. 10. In the in-line direction, a lower bound of 1 Hz ($0.37 f_{n1}$) is imposed to manifest the high-frequency components, otherwise their effects will be overshadowed by the low-frequency, large-amplitude in-line oscillation. It is shown that the first-order modal vibration near the motion reversal is at the first natural frequency while the second-order modal vibration at the second natural frequency dominates the whole cylinder. In contrast, nearly no first-natural-frequency-dominated stages are found for the in-line hydrodynamic forces.

Similar figures in the cross-flow direction are presented in Fig. 11. From the cross-flow displacement figure, the build-up – lock-in – die-out cycle features can be clearly observed. The die-out stages appear to be longer than the build-up stages, forming a triangle-shaped envelope pointing to the right for each cycle. Actually, the cross-flow amplitude is still decreasing when the cylinder starts to accelerate. Though the lag also exists for the amplitude peaks, it is not as evident, resulting in longer decreasing amplitude stages. This conclusion fits Figs. 5 and 6. It can be seen from these two figures that the amplitude is actually decreasing at the beginning of the accelerating stages. The peak amplitude of the oscillations in the cross-flow hydrodynamic coefficient is not a stable value. As is seen, it varies from one period to another. It may even happen that peaks in some periods are missed, such as $t \cdot T_w^{-1} = 11$. From the modal weights it is clearly seen that the second-order modal weight for the cross-flow hydrodynamic forces is more pronounced than the cross-flow displacements. This can be due to that forces are more sensitive to any small changes in the flow, especially to high-frequency fluctuations, while displacements as the

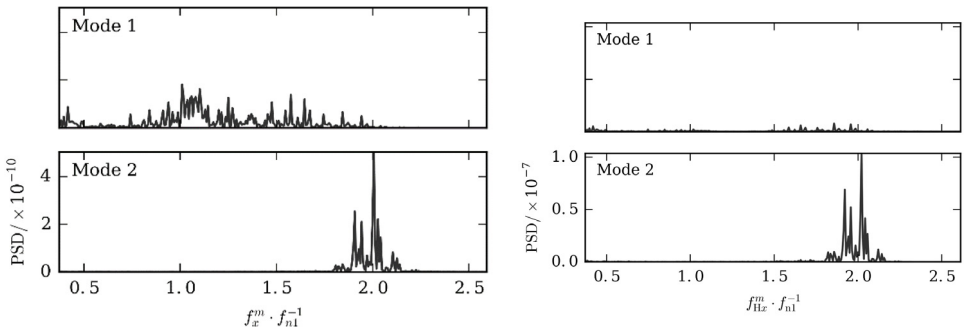

Fig. 10. Power spectral density of modal weights of the relative in-line displacements $x \cdot D^{-1}$ and the in-line hydrodynamic force coefficients C_{Hx} over the entire cylinder. The in-line modal vibration frequencies f_x^m and the in-line modal hydrodynamic force frequencies f_{Hx}^m are non-dimensionalized by the first natural frequency f_{n1}.

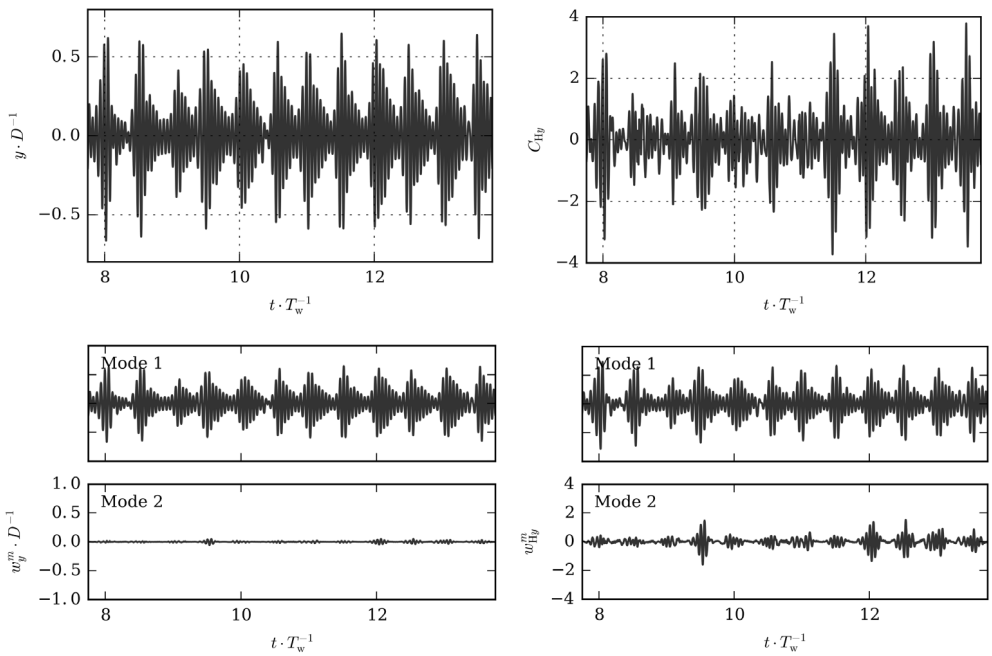

Fig. 11. The cross-flow displacements $y \cdot D^{-1}$ and the cross-flow hydrodynamic force coefficients C_{Hy} at the mid-span of the cylinder (upper) and modal weights of $y \cdot D^{-1}$ and C_{Hy} over the entire cylinder, $w_y^m \cdot D^{-1}$ and w_{Hy}^m (lower).

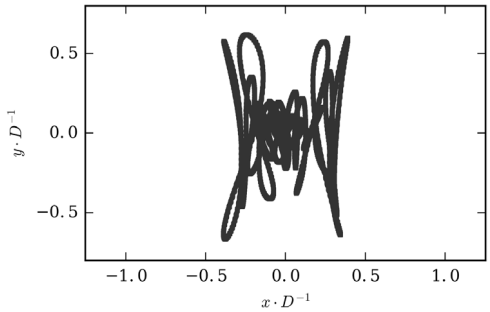

Fig. 12. The trajectory of vibrations at the mid-span of the cylinder. The support motion is not included in the in-line displacement.

result of the actions of forces over a short period of time. This cumulative effect inevitably renders displacements more stable.

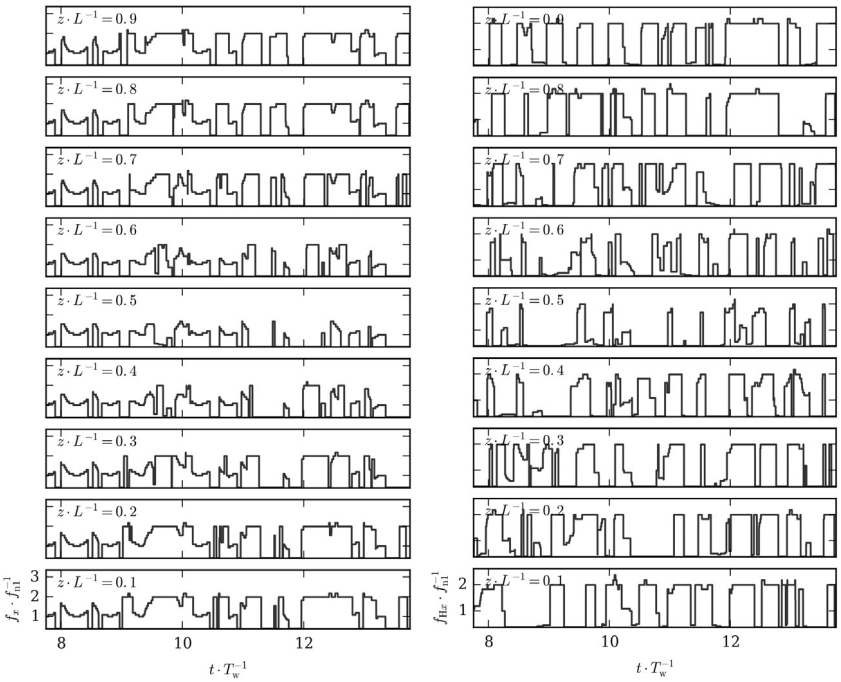

Fig. 13. Wavelet analyses of the in-line displacements x and of the in-line hydrodynamic force coefficients C_{Hx}.

The trajectory of the vibrations in an oscillatory period is plotted in Fig. 12. The two '8' figures are located at two sides of the trajectory, in accordance with the above analyses that the most intense vibrations in both directions occur when the relative in-line displacement reaches its extreme value, during which the first natural frequency dominates the cross-flow vibrations while the second natural frequency dominates the in-line vibration. The in-line vibration is mainly at the first natural frequency when relative in-line displacement gets close to zero. This may explain the small circular coils in the center. The butterfly-shaped trajectory can be a key feature of vibrations of flexible cylinders in oscillatory flows in low-mode cases.

The dominant vibration frequencies of the displacements and force coefficients varying over time obtained from wavelet analyses are given in Fig. 13 for in-line direction and Fig. 14 for cross-flow direction. Fig. 13 clearly presents three states the cylinder experiences in the in-line direction: the first-natural-frequency vibration dominated stage, the second-natural-frequency vibration dominated stage, and the lower-frequency oscillation dominated stage (despite that a lower bound of 1 Hz is imposed). The first natural frequency rather than the second natural frequency dominates the in-line vibrations at $z \cdot L^{-1} = 0.5$, for that the mid-span of the cylinder is exactly the standing point of the second mode. On the other hand, near the two sides the cylinder is less likely to vibrate at the first natural frequency. However, almost no such first-natural-frequency vibration dominated stages occur in the force figure, as formerly shown in Fig. 10, indicating that the displacements and the hydrodynamic forces are dominated by different frequencies and lock in does not occur at the mid-span in the in-line direction. No lock-in means less stable forces. As a result of this, the in-line hydrodynamic force coefficient at the mid-span is dominated by the low-frequency oscillation for the most time. The subject can probably be best explained by that no standing points of forces exist along the span. Once vortex shedding occurs, the generated forces appear, no matter whether the displacement at the position is zero (at twice the Strouhal frequency for the in-line hydrodynamic forces of a stationary cylinder). No lock-in only means less amplitude for the forces, which is exactly the case for the in-line hydrodynamic force at the mid-span of the cylinder. Frequencies being out of sync also appears near two ends of the cylinder where the displacements are very limited. Near the peaks or valleys of the second-order mode, i.e. $z \cdot L^{-1} = 0.25, 0.75$, lock-in occurs, resulting in the almost same frequency at the same time between the displacements and the forces and large amplitudes for both. When we look back at Fig. 8 it will be seen that the more obvious high-frequency fluctuations and instabilities in in-line hydrodynamic force coefficients may be attributed to both the more sensitive nature to the short-period changes as well as the non-lock-in state.

The frequencies of the cross-flow vibrations are much more stable. The slight fluctuations of the vibration frequencies would presumably be due to the variation of the natural frequency with the reduced velocity, considering that the mass ratio is merely 1.53. The natural frequency in the water situation is not maintained at its still-water value, but rather it increases with the reduced velocity (Sumer and Fredsøe, 1997). Different from the stable displacements, the cross-flow hydrodynamic force frequencies occasionally experience an abrupt drop to some frequency lower than the first natural frequency but larger than the lower bound of 1 Hz, especially near two ends of the cylinder. This suggests that the displacements lose control over

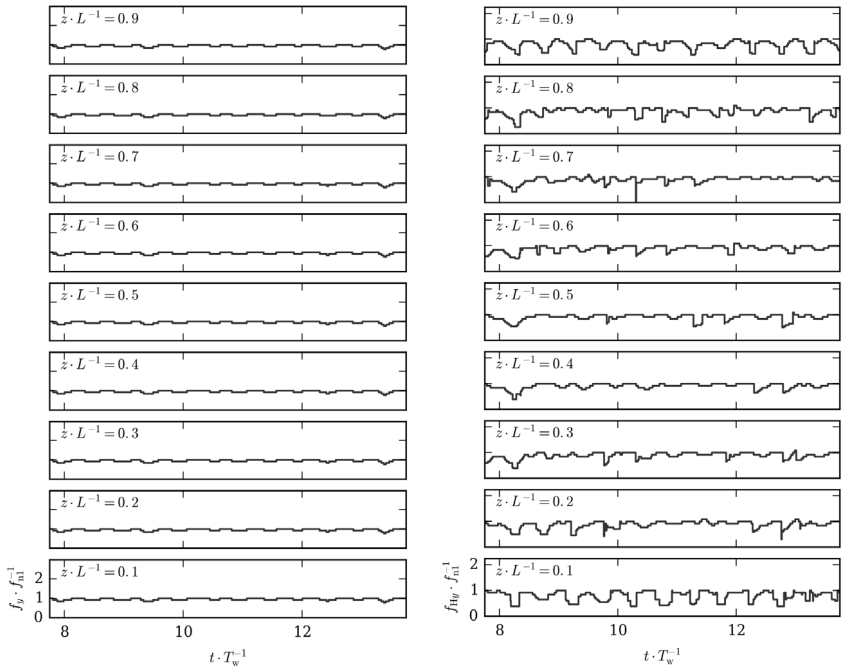

Fig. 14. Wavelet analyses of the cross-flow displacements y and of the cross-flow hydrodynamic force coefficients C_{Hy}.

the forces near the two ends due to small vibration amplitudes. The displacement and force frequency diagrams indicate that the small-amplitude vibrations occur at the first natural frequency, while the vortex shedding (the fluctuations in the cross-flow hydrodynamic forces) mainly occurs at the stationary cylinder Strouhal frequency, going up and down, in exactly the same fashion as for rigid cylinders (Sumer and Fredsøe, 1997). While near the mid-span the vortex shedding is controlled by the Strouhal law in lesser time.

5. Conclusions

The vortex-induced vibrations of a flexible cylinder oscillating harmonically in still water with *KC* of 84 have been numerically simulated using a CFD method. The simulation results have been compared with a test carried out by Wang et al. (2014) and further analyzed. One feature of the vortex-induced vibrations in oscillatory flows is the build-up – lock-in – die-out cycle. The hysteresis between the decelerating and the accelerating stages is another distinct feature. The in-line vibrations in the present low-mode case consist of three components, the low-frequency oscillation, the first-natural-frequency vibration during the cylinder reversal, and the second-natural-frequency vibration due to vortex shedding. The first natural frequency component during the cylinder reversal deserves further research. The trajectory turns out to be butterfly-shaped, the two '8' figures indicating that the frequency of in-line vibration during lock-in stage is twice that of cross-flow vibration, and the lock-in occurs when the cylinder reaches its maximum in-line displacement. Detailed wavelet analyses of the vibrations have been given. It is shown that the first natural frequency is less likely to dominate the in-line hydrodynamic forces, even at the mid-span of the cylinder, where the in-line vibrations are dominated by the first natural frequency.

Acknowledgments

This work is supported by the National Natural Science Foundation of China (51490675, 51379125, 11432009, 51579145), Chang Jiang Scholars Program (T2014099), Shanghai Excellent Academic Leaders Program (17XD1402300), Program for Professor of Special Appointment (Eastern Scholar) at Shanghai Institutions of Higher Learning (2013022), Innovative Special Project of Numerical Tank of Ministry of Industry and Information Technology of China (2016-23/09) and Lloyd's Register Foundation for doctoral student, to which the authors are most grateful.

References

Anagnostopoulos, P., Iliadis, G., 1998. Numerical study of the flow pattern and the in-line response of a flexible cylinder in an oscillating stream. J. Fluids Struct. 12, 225–258. http://dx.doi.org/10.1006/jfls.1997.0139.

Blevins, R., 2001. Flow-Induced Vibration, second ed. Krieger Publishing Company, Malabar, Florida.
Chien, K., 1982. Predictions of channel and boundary-layer flows with a low-Reynolds-number turbulence model. AIAA J. 20, 33–38.
Clough, R.W., Penzien, J., 2003. Dynamics of Structures, third ed. Computers & Structures, Inc., Berkeley.
Duan, M., Wan, D.C., Xue, H., 2016. Prediction of response for vortex-induced vibrations of a flexible riser pipe by using multi-strip method. In: Proceedings of the Twenty-sixth (2016) International Ocean and Polar Engineering Conference Rhodes, Greece, June 26–July 1, pp. 1065–1073.
Fu, B., Duan, M., Wan, D.C., 2016. Effect of mass ratio on the vortex-induced vibrations of a top tensioned riser. In: The Second Conference of Global Chinese Scholars on Hydrodynamics Effect, Wuxi, China, pp. 431–435.
Graham, J.M.R., Djahansouz, B., 1991. Computation of vortex shedding from rigid and compliant cylinders in waves. In: Proceedings of the First (1991) International Offshore and Polar Engineering Conference. The International Society of Offshore and Polar Engineers, Edinburgh, United Kingdom, pp. 504–508.
Holzmann, T., 2017. Mathematics, Numerics, Derivations and OpenFOAM(R), fourth ed. Holzmann-cfd.
Jasak, H., 2009. Dynamic mesh handling in OpenFOAM. In: 47th AIAA Aerospace Sciences Meeting Including the New Horizons Forum and Aerospace Exposition. American Institute of Aeronautics and Astronautics, Inc., Orlando, Floridaspace. http://dx.doi.org/10.2514/6.2009-341.
Kozakiewicz, A., Sumer, B.M., Fredsøe, J., 1992. Spanwise correlation on a vibrating cylinder near a wall in oscillatory flows. J. Fluids Struct. 6, 371–392.
Kozakiewicz, A., Sumer, B.M., Fredsøe, J., 1994. Cross-flow vibrations of cylinder in irregular oscillatory flow. J. Waterw. Port, Coastal, Ocean Eng. 120, 515–534. http://dx.doi.org/10.1061/(ASCE)0733-950X(1996)122:3(155).
Kozakiewicz, A., Sumer, B.M., Fredsøe, J., Hansen, E.A., 1997. Vortex regimes around a freely vibrating cylinder in oscillatory flow. Int. J. Offshore Polar Eng. 7, 94–103.
Lie, H., Kaasen, K.E., 2006. Modal analysis of measurements from a large-scale VIV model test of a riser in linearly sheared flow. J. Fluids Struct. 22, 557–575. http://dx.doi.org/10.1016/j.jfluidstructs.2006.01.002.
Lipsett, A.W., Williamson, J.D., 1991. Modelling the response of flexibly mounted cylinders in oscillatory flow. In: Proceedings of the First (1991) International Offshore and Polar Engineering Conference. The International Society of Offshore and Polar Engineers, Edinburgh, United Kingdom, pp. 11–16.
Menter, F.R., 1994. Two-equation Eddy-viscosity turbulence models for engineering applications. AIAA J. 32, 1598–1605. http://dx.doi.org/10.2514/3.12149.
Menter, F.R., Kuntz, M., Langtry, R., 2003. Ten years of industrial experience with the SST turbulence model. In: Hanjalic, K., Nagano, Y., Tummers, M. (Eds.), Turbulence, Heat and Mass Transfer, vol. 4. Begell House Inc.
Sarpkaya, T., 1979. Vortex-induced oscillations - A selective review. J. Appl. Mech. 46, 241–258.
Sarpkaya, T., 1986. Force on a circular cylinder in viscous oscillatory flow at low Keulegan–Carpenter numbers. J. Fluid Mech. 165, 61–71. http://dx.doi.org/10.1017/S0022112086002999.
Sumer, B.M., Fredsøe, J., 1988. Transverse vibrations of an elastically mounted cylinder exposed to an oscillating flow. J. Offshore Mech. Arct. Eng. 110, 387–394.
Sumer, B.M., Fredsøe, J., 1997. Hydrodynamics Around Cylindrical Structures. World Scientific, singapore.
Trim, A.D., Braaten, H., Lie, H., Tognarelli, M.A., 2005. Experimental investigation of vortex-induced vibration of long marine risers. J. Fluids Struct. 21, 335–361. http://dx.doi.org/10.1016/j.jfluidstructs.2005.07.014.
Wan, D.C., Duan, M.Y., 2017. A recent review of numerical studies on vortex-induced vibrations of long slender flexible risers in deep sea. Chinese Quart. Mech. 28 (2), 179–196.
Wang, J., Fu, S., Xu, Y., Song, L., 2014. Viv developing process of a flexible cylinder under oscillatory flow. Chin. J. Theor. Appl. Mech. 46, 173–182. http://dx.doi.org/10.6052/0459-1879-13-277.
Wilcox, D.C., 1993. Turbulence Modeling for CFD. DCW Industries, Inc., La Canada, California.
Willden, R.H.J., Graham, J.M.R., 2004. Multi-modal vortex-induced vibrations of a vertical riser pipe subject to a uniform current profile. Eur. J. Mech. B Fluids 23, 209–218. http://dx.doi.org/10.1016/j.euromechflu.2003.09.011.
Zhao, M., 2013. Numerical investigation of two-degree-of-freedom vortex-induced vibration of a circular cylinder in oscillatory flow. J. Fluids Struct. 39, 41–59. http://dx.doi.org/10.1016/j.jfluidstructs.2013.02.003.